

Laser spectroscopy of $(\nu=0, R=1)10F$ and $(\nu=0, R=1)10G$ states of H_2 : A test of the polarization model

W. G. Sturuss, E. A. Hessels, P. W. Arcuni, and S. R. Lundeen
Department of Physics, University of Notre Dame, Notre Dame, Indiana 46556
 (Received 3 December 1987; revised manuscript received 26 February 1988)

Rydberg states of H_2 consisting of a $10F$ or $10G$ electron bound to the $\nu=0, R=1$ state of H_2^+ are studied using Doppler-tuned laser spectroscopy of Rydberg-Rydberg transitions. The positions of all such states are measured to a precision of better than 0.01 cm^{-1} and are compared with the predictions of the polarization model. The polarization model is derived from first principles. Nonadiabatic corrections to the dipole polarization energies, calculated for the first time, are found to be expressible in terms of the S_{-3} -moment functions of H_2^+ . Higher-order adiabatic polarization energies are estimated from calculated higher-order H_2^+ polarizabilities.

I. INTRODUCTION

In recent years, new experimental techniques have made possible the first observations of a new class of electronically excited states of H_2 , the Rydberg states with large values of the orbital angular momentum ($L \geq 3$).¹⁻³ The structure of these states is found to be very different from excited states with lower L . In particular, they conform closely to an "atomlike" coupling scheme in which the angular momentum of the Rydberg electron (L) and the total angular momentum of the H_2^+ ion core (R) are both good quantum numbers, coupling together according to the usual rules of angular momentum addition to form $N=R+L$, the total angular momentum of the system (exclusive of spin).⁴ The H_2^+ ion rotates freely within the orbit of the Rydberg electron, acting much like an atomic nucleus with spin R . Following Ref. 1, we refer to these states with the notation $(\nu, R)nL_N$, where ν is the vibrational quantum number of the core and n is the principle quantum number of the Rydberg electron. The wave functions of these states are closely approximated by a product of eigenstates of the free H_2^+ ion and of the hydrogenic Rydberg electron. Because both parts of this system can be understood separately with great precision, and since the coupling between them is weak, these states of the H_2 molecule should be amenable to unusually precise theoretical description.

The highest-resolution experimental studies of these states to date have been obtained using microwave spectroscopy on a fast beam of Rydberg states.⁵ Systematic and extensive microwave spectroscopy in such states appears feasible with this technique and should soon result in dramatic improvements in the precision with which these structures are known. Eventually it may be possible to infer from such measurements new precise information about the H_2^+ ion. With this in mind, it appears desirable to improve the precision of the optical spectroscopy reported in Ref. 1 to the point where higher-order corrections to the simple Rydberg fine-structure model used there become significant. We report here improved spectroscopy of the $(0,1)10F$ and $(0,1)10G$ states of H_2 ,

which establishes their positions to a precision of better than $\pm 0.01 \text{ cm}^{-1}$ and allows a more precise comparison with theory.

In Sec. II the theory of these high- L Rydberg states is discussed and expressions for both adiabatic and nonadiabatic parts of the dipole polarization energies are derived. The effects of higher-order adiabatic polarizabilities on the structure of the system are discussed, and the most important uncalculated terms in a systematic polarization model of H_2 Rydberg structure are identified. In Sec. III the improved measurements of the $(0,1)10F$ and $(0,1)10G$ states are described. In Sec. IV the results are compared with theory and conclusions are drawn.

II. POLARIZATION MODEL FOR H_2 RYDBERG STATES

Experiments have shown that the high- L Rydberg states of H_2 are described, at least approximately, by a simple polarization model in which the deviation from the hydrogenic structure is given by the expectation value of

$$V_{\text{eff}} = -\frac{eQ(\rho)}{r^3} P_2(\cos\theta) - \frac{1}{2} \frac{e^2}{r^4} \alpha_s(\rho) - \frac{1}{3} \frac{e^2}{r^4} \alpha_T(\rho) P_2(\cos\theta), \quad (1)$$

where Q is the quadrupole moment, α_s and α_T are the isotropic and anisotropic dipole polarizabilities of the H_2^+ core (each being functions of the internuclear separation ρ), θ is the angle between the internuclear axis and the Rydberg electron's position, and r is the radial coordinate of the Rydberg electron. The expectation value is over a reduced wave function,

$$\psi_{\nu R n L N}^{\text{Ryd}} = g_{\nu R} \frac{(\rho)}{\rho} \sum_{M, m_1} \langle R, M, L, m_1 | R, L, N, m \rangle \times Y_{RM}(\hat{\rho}) \psi_{n L m_1}(\mathbf{r}), \quad (2)$$

which has no dependence on the coordinate of the core electron. All dependence on the core electronic structure is contained in the coefficients Q , α_s , and α_T . We refer to this model as the lowest-order polarization model (LOPM). It was apparently first discussed by Jungen and Miescher in connection with their description of Rydberg states of NO,⁶ and has since been used by several workers to describe Rydberg states of H₂.^{1-3,5,7-10} Some aspects of the theoretical justification for this approach were discussed by Eyler and Pipkin,⁷ but the polarization terms have apparently never been derived from first principles. In order to assess more carefully the limitations of this model, such a derivation is provided in the following. The expectation value of the potential of Eq. (1) lifts the hydrogenic degeneracy of the zeroth-order states, giving rise to a fine structure which is typically 10⁻³ of the energy spacing between adjacent zeroth-order states. We refer to this structure as electric fine structure (EFS) since it is totally due to Coulomb forces. A finer level of structure due to the inclusion of spins, the magnetic fine structure (MFS), has been discussed elsewhere⁵ and will not be treated here.

A good share of the motivation for applying the polarization model to high- L Rydberg states of H₂ is derived from the success that has been achieved in describing similar states in the helium atom with this approach.^{11,12} These studies suggest the adoption of two basic assumptions, which have been shown to be good approximations in the case of high- L states of the helium atom,¹¹ and which, in any case, become more nearly valid as L increases.

(1) The two electrons are *distinguishable*. Electron 2 is the Rydberg electron.

(2) There is *no penetration* of the wave function of the core electron by the Rydberg electron.

In adopting these assumptions, the possibility of calculating the electronic exchange energy is forfeited, but since the exchange energy is expected to be small in those high- L states,¹³ this is not a major limitation. Small energy shifts due to core penetration are also neglected in this approach.¹¹

The Hamiltonian for the system may be written as

$$H = H_0 + V, \quad (3)$$

where

$$H_0 = \left[\frac{|\mathbf{P}_1|^2}{2M} + \frac{|\mathbf{P}_2|^2}{2M} + \frac{|\mathbf{p}_{e1}|^2}{2m} - \frac{e^2}{|\mathbf{r}_{e1} - \mathbf{R}_1|} \right. \\ \left. - \frac{e^2}{|\mathbf{r}_{e1} - \mathbf{R}_2|} + \frac{e^2}{|\mathbf{R}_2 - \mathbf{R}_1|} \right] \\ + \left[\frac{|\mathbf{p}_{e2}|^2}{2m} - \frac{e^2}{|\mathbf{r}_{e2} - (\mathbf{R}_1 + \mathbf{R}_2)/2|} \right]$$

and

$$V = e^2 \left[\frac{1}{|\mathbf{r}_{e2} - (\mathbf{R}_1 + \mathbf{R}_2)/2|} + \frac{1}{|\mathbf{r}_{e2} - \mathbf{r}_{e1}|} \right. \\ \left. - \frac{1}{|\mathbf{r}_{e2} - \mathbf{R}_1|} - \frac{1}{|\mathbf{r}_{e2} - \mathbf{R}_2|} \right],$$

where \mathbf{r}_{e1} is the coordinate of the electron 1, \mathbf{R}_1 is the coordinate of proton 1, etc., and m and M represent the electron and proton masses. Introducing the relative coordinates

$$\mathbf{R}_c \equiv (\mathbf{R}_1 + \mathbf{R}_2)/2, \quad \boldsymbol{\rho} \equiv \mathbf{R}_2 - \mathbf{R}_1,$$

$$\mathbf{r}_1 \equiv \mathbf{r}_{e1} - \mathbf{R}_c, \quad \mathbf{r}_2 \equiv \mathbf{r}_{e2} - \mathbf{R}_c$$

and neglecting mass-polarization terms, H_0 can be rewritten as

$$H_0 = \frac{|\mathbf{P}_c|^2}{4M} + \left[\frac{|\mathbf{P}_\rho|^2}{M} + \frac{|\mathbf{p}_1|^2}{2\mu} - \frac{e^2}{|\mathbf{r}_1 - \boldsymbol{\rho}/2|} \right. \\ \left. - \frac{e^2}{|\mathbf{r}_1 + \boldsymbol{\rho}/2|} + \frac{e^2}{|\boldsymbol{\rho}|} \right] \\ + \left[\frac{|\mathbf{p}_2|^2}{2\mu} - \frac{e^2}{|\mathbf{r}_2|} \right], \quad (4)$$

where $\mu = 2Mm/(m + 2M)$ and V can be written as

$$V = e^2 \left[\frac{1}{|\mathbf{r}_2|} + \frac{1}{|\mathbf{r}_2 - \mathbf{r}_1|} - \frac{1}{|\mathbf{r}_2 - \boldsymbol{\rho}/2|} \right. \\ \left. - \frac{1}{|\mathbf{r}_2 + \boldsymbol{\rho}/2|} \right]. \quad (5)$$

The eigenstates of H_0 are products of eigenstates of the nuclear center-of-mass momentum (which we henceforth neglect), the hydrogenic Rydberg electron (\mathbf{r}_2), and the free H₂⁺ ion. In the Born-Oppenheimer approximation, the H₂⁺ eigenstates can be written as

$$\psi_{\alpha\Lambda\nu RM}^0(\boldsymbol{\rho}, \mathbf{r}_1) = \frac{g_{\alpha\Lambda\nu R}(\boldsymbol{\rho})}{\rho} f_{\alpha\Lambda}(\mathbf{r}'_1; \boldsymbol{\rho}) \left[\frac{2R + 1}{4\pi} \right]^{1/2} \\ \times d_{\Lambda M}^R(\theta) e^{iM\phi}, \quad (6)$$

where α and Λ ($=\mathbf{L}_1 \cdot \hat{\boldsymbol{\rho}}$) specify the electronic state, \mathbf{R} is the total angular momentum (exclusive of spin), ν is the vibrational quantum number, and θ and ϕ are the polar coordinates of $\hat{\boldsymbol{\rho}}$ in the laboratory. The coordinate \mathbf{r}'_1 is defined with respect to the rotated coordinate system which has $\hat{\mathbf{z}}' \parallel \hat{\boldsymbol{\rho}}$. The functions $d_{\Lambda M}^R(\theta)$ are related to representations of finite rotations¹⁴ and are expressed in the notation of Edmonds.¹⁵

The vector coupled eigenstates of total angular momentum

$$\mathbf{N} = \mathbf{R} + \mathbf{L}$$

are given by

$$\begin{aligned} \psi_{\alpha\Lambda\nu RnLNm}^0(\boldsymbol{\rho}, \mathbf{r}_1, \mathbf{r}_2) &= \sum_{M, m_1} \langle R, M, L, m_1 | R, L; N, m \rangle \\ &\times \psi_{\alpha\Lambda\nu RM}^0(\boldsymbol{\rho}, \mathbf{r}_1) \\ &\times \psi_{nLm_1}^0(\mathbf{r}_2). \end{aligned} \quad (7)$$

The assumption of no penetration may be expressed as $r_2 > r_1$ and $r_2 > \rho/2$. For sufficiently high- L Rydberg states these relations will be satisfied for all parts of the configuration space $(\mathbf{r}_1, \mathbf{r}_2, \boldsymbol{\rho})$ where the wave function is nonnegligible. Using these relations, the perturbation V can be written as

$$\begin{aligned} \langle X\nu RnLNm | V | X\nu R'n'L'Nm \rangle &= e^2 \sum_{\kappa=1}^{\infty} (-1)^{N+L+R'} \begin{Bmatrix} R' & L' & N \\ L & R & \kappa \end{Bmatrix} \left\langle nL \left\| \frac{C^\kappa(\Omega_2)}{r_2^{\kappa+1}} \right\| n'L' \right\rangle \\ &\times \{ \langle X\nu R \| r_1^\kappa C^\kappa(\Omega_1) \| X\nu R' \rangle \\ &- [1 + (-1)^\kappa] \langle X\nu R \| (\rho/2)^\kappa C^\kappa(\hat{\boldsymbol{\rho}}) \| X\nu R' \rangle \}, \end{aligned} \quad (9)$$

where

$$\begin{aligned} \left\langle nL \left\| \frac{C^\kappa(\Omega_2)}{r_2^{\kappa+1}} \right\| n'L' \right\rangle &= (-1)^L [(2L+1)(2L'+1)]^{1/2} \\ &\times \begin{Bmatrix} L & \kappa & L' \\ 0 & 0 & 0 \end{Bmatrix} \\ &\times \left[nL \left\| \frac{1}{r_2^{\kappa+1}} \right\| n'L' \right], \end{aligned} \quad (10)$$

with

$$[nL \| r^s \| n'L'] \equiv \int_0^\infty P_{nL}(r) P_{n'L'}(r) r^s dr.$$

$C^\kappa(\Omega)$ is the spherical tensor of rank κ ¹⁵ and $P_{nL}(r)$ is r times the radial part of the hydrogenic wave function. The reduced matrix elements of the operator $r_1^\kappa C^\kappa(\Omega_1)$ can be evaluated using the transformation properties of the spherical tensors,

$$C_q^\kappa(\Omega_1) = \sum_q D_{q'q}^\kappa(0, -\theta, -\phi) C_{q'}^\kappa(\Omega_1') \quad (11)$$

(where Ω_1 denotes the angular coordinates of electron 1 in the laboratory and Ω_1' its angular coordinates in the molecule fixed coordinate system), along with the fact that

$$\begin{aligned} \int_0^\pi d_{aa'}^A(\theta) d_{bb'}^B(\theta) d_{cc'}^C(\theta) \sin\theta d\theta \\ = 2 \begin{Bmatrix} A & B & C \\ a & b & c \end{Bmatrix} \begin{Bmatrix} A & B & C \\ a' & b' & c' \end{Bmatrix}. \end{aligned} \quad (12)$$

$$\begin{aligned} V &= e^2 \sum_{\kappa=1}^{\infty} \frac{r_1^\kappa}{r_2^{\kappa+1}} P_\kappa(\cos\theta_{21}) \\ &- [1 + (-1)^\kappa] \frac{(\rho/2)^\kappa}{r_2^{\kappa+1}} P_\kappa(\cos\theta_{2\rho}), \end{aligned} \quad (8)$$

where θ_{21} is the angle between \mathbf{r}_1 and \mathbf{r}_2 and $\theta_{2\rho}$ is the angle between \mathbf{r}_2 and $\boldsymbol{\rho}$. The matrix element of each term of this multipole expansion can be evaluated with standard angular momentum methods.¹⁵

The Rydberg-state energy may be calculated systematically using perturbation theory, starting with the set of zeroth-order states of the form of Eq. (7) and using the perturbation V [Eq. (8)]. Of particular importance in this calculation are those matrix elements of V which are diagonal in the core electronic state, especially when that common electronic state is the ground electronic state of H_2^+ ($X^2\Sigma_g^+$), which we denote here by $\alpha\Lambda = X$. In this case the result is

The result is

$$\begin{aligned} \langle X\nu R \| r_1^\kappa C^\kappa(\Omega_1) \| X\nu R' \rangle \\ = (-1)^R [(2R+1)(2R'+1)]^{1/2} \begin{Bmatrix} R & \kappa & R' \\ 0 & 0 & 0 \end{Bmatrix} \\ \times \int_0^\infty g_{X\nu R}(\rho) Q_e^\kappa(\rho) g_{X\nu R'}(\rho) d\rho, \end{aligned} \quad (13)$$

where

$$Q_e^\kappa(\rho) = \int |f_X(\mathbf{r}_1; \rho)|^2 C_0^\kappa(\Omega_1') r_1^\kappa d^3r_1.$$

Note that because of the reflection symmetry of the electronic wave function $Q_e^\kappa(\rho) = 0$ for all odd κ .

By explicit calculation with functions of the form of Eq. (6), it can also be shown that

$$\begin{aligned} \langle X\nu R \| (\rho/2)^\kappa C^\kappa(\hat{\boldsymbol{\rho}}) \| X\nu R' \rangle \\ = (-1)^R [(2R+1)(2R'+1)]^{1/2} \begin{Bmatrix} R & \kappa & R' \\ 0 & 0 & 0 \end{Bmatrix} \\ \times \int g_{X\nu R}(\rho) (\rho/2)^\kappa g_{X\nu R'}(\rho) d\rho. \end{aligned} \quad (14)$$

Thus the full result for matrix elements of V diagonal in the ground electronic state of H_2^+ is

$$\begin{aligned} \langle X\nu RnLNm | V | X\nu'R'n'L'Nm \rangle &= -e^2 \sum_{\kappa=2,4,\dots}^{\infty} (-1)^N \begin{Bmatrix} R' & L' & N \\ L & R & \kappa \end{Bmatrix} \begin{Bmatrix} R & \kappa & R' \\ 0 & 0 & 0 \end{Bmatrix} \begin{Bmatrix} L & \kappa & L' \\ 0 & 0 & 0 \end{Bmatrix} \\ &\times [(2R+1)(2R'+1)(2L+1)(2L'+1)]^{1/2} \\ &\times \left[nL \left| \left| \frac{1}{r^{\kappa+1}} \right| \right| n'L' \right] \int g_{X\nu R}(\rho) Q^\kappa(\rho) g_{X\nu'R'}(\rho) d\rho, \end{aligned}$$

where

$$Q^\kappa(\rho) \equiv 2(\rho/2)^\kappa - Q_e^\kappa(\rho). \quad (15)$$

These matrix elements may be written in terms of an effective potential

$$\begin{aligned} U(\rho, \mathbf{r}_2) &= \sum_{\kappa=2,4,\dots}^{\infty} U^\kappa(\rho, \mathbf{r}_2) \\ &= \sum_{\kappa=2,4,\dots}^{\infty} \frac{-e^2 Q^\kappa(\rho)}{r_2^{\kappa+1}} P_\kappa(\cos\theta_{2\rho}), \end{aligned} \quad (16)$$

which gives

$$\begin{aligned} \langle X\nu RnLNm | V | X\nu'R'n'L'Nm \rangle \\ = \langle \psi_{\nu RnLN}^{\text{Ryd}} | U(\rho, \mathbf{r}_2) | \psi_{\nu'R'n'L'N}^{\text{Ryd}} \rangle, \end{aligned} \quad (17)$$

with $\psi_{\nu RnLN}^{\text{Ryd}}$ given by Eq. (2).

Using this result, the first-order perturbation energies can be written as

$$\begin{aligned} E^{[1]}(X\nu RnLN) \\ = \left\langle \psi_{\nu RnLN}^{\text{Ryd}} \left| \sum_{\kappa=2,4,\dots} U^\kappa(\rho, \mathbf{r}_2) \right| \psi_{\nu RnLN}^{\text{Ryd}} \right\rangle. \end{aligned} \quad (18)$$

The first term ($\kappa=2$) in this expansion in the permanent multipole moments of H_2^+ is just the quadrupole term in Eq. (1). The next nonzero moment ($\kappa=4$) is the hexadecapole moment. This and higher moments can contribute to the energy of a particular Rydberg state only if both L and R are sufficiently large, so that the $6j$ symbol in Eq. (15) is nonzero. If J is the lesser of R and L , then a given κ can contribute only if it satisfies the triangle inequality

$$\Delta(J, J, \kappa) \neq 0.$$

In the particular case of $R=1$ states, which is studied in the following, only the quadrupole term has a nonzero expectation value.

The second-order perturbation energies are given by

$$E^{[2]}(X\nu RnLN) = \sum_{\alpha, \Lambda, \nu', R', n', L'} \frac{|\langle X\nu RnLNm | V | \alpha \Lambda \nu' R' n' L' Nm \rangle|^2}{E^0(X\nu Rn) - E^0(\alpha \Lambda \nu' R' n')}. \quad (19)$$

This expression separates naturally into two parts, depending on whether electron 1 (the core electron) remains in its ground electronic state in the intermediate state. If it does, setting $\alpha\Lambda=X$, this part of Eq. (19) can be written, using Eq. (17), as

$$\begin{aligned} E_X^{[2]}(X\nu RnLN) \\ = \sum_{\nu', R', n', L'} \frac{|\langle \psi_{\nu RnLN}^{\text{Ryd}} | U(\rho, \mathbf{r}_2) | \psi_{\nu'R'n'L'N}^{\text{Ryd}} \rangle|^2}{E^0(X\nu Rn) - E^0(X\nu'R'n')}, \end{aligned} \quad (20)$$

and represents the effect of mixing between different Ryd-

berg series. Energy shifts due to such mixing are quite significant for Rydberg states of low L ,^{16,7} but decrease rapidly as L increases. In addition to their effects on the Rydberg state energies, these mixings are also responsible for vibrational and rotational autoionization via long-range interactions in high- L Rydberg states.¹⁷

The part of the second-order energy [Eq. (19)] coming from intermediate states, where the core electron is not in its ground electronic states, leads to the polarization potential, the leading terms of which are the adiabatic dipole polarization terms shown in Eq. (1). The separation between "adiabatic" and "nonadiabatic" terms in this context is based on an expansion of the energy denominator in Eq. (19),

$$\begin{aligned} \frac{1}{E^0(X\nu Rn) - E^0(\alpha \Lambda \nu' R' n')} &= \frac{1}{[E^0(X\nu R) - E^0(\alpha \Lambda \nu' R')] + [E^0(n) - E^0(n')]} \\ &\cong \frac{1}{E^0(X\nu R) - E^0(\alpha \Lambda \nu' R')} - \frac{E^0(n) - E^0(n')}{[E^0(X\nu R) - E^0(\alpha \Lambda \nu' R')]^2} + \dots \end{aligned} \quad (21)$$

The first term in Eq. (21) gives the adiabatic polarization energies, while the second gives the first "nonadiabatic" corrections.

For the portion of the second-order perturbation energy due to electronically excited core states, the second term in Eq. (8) does not contribute because of the orthogonality of core electronic states. Successive terms in the multipole expansion of the first term produce effective potentials proportional to increasingly higher inverse powers of r_2 . We consider here only the contributions from the lowest-order term in V , the dipole term. Evaluation of these terms requires the matrix element

$$\begin{aligned} \left\langle X\nu R n L N m \left| \frac{e^2 r_1}{r_2^2} C^1(\Omega_1) C^1(\Omega_2) \right| \alpha \Lambda \nu' R' n' L' N m \right\rangle = e(-1)^{N+L+R'} \begin{Bmatrix} R' & L' & N \\ R & L & 1 \end{Bmatrix} \langle X\nu R \| e r_1 C^1(\Omega_1) \| \alpha \Lambda \nu' R' \rangle \\ \times \langle n L \| C^1(\Omega_2) / r_2^2 \| n' L' \rangle, \end{aligned} \quad (22)$$

where

$$\begin{aligned} \langle X\nu R \| e r_1 C^1(\Omega_1) \| \alpha \Lambda \nu' R' \rangle = (-1)^R [(2R+1)(2R'+1)]^{1/2} \begin{Bmatrix} R & 1 & R' \\ 0 & -\Lambda & \Lambda \end{Bmatrix} \\ \times \int_0^\infty g_{X\nu R}(\rho) D_{X,\alpha\Lambda}(\rho) g_{\alpha\Lambda\nu'R'}(\rho) d\rho, \end{aligned}$$

with

$$D_{X,\alpha\Lambda}(\rho) \equiv e \int f_X^*(\mathbf{r}'_1; \rho) r_1 C_{-\Lambda}^1(\Omega'_1) f_{\alpha\Lambda}(\mathbf{r}'_1; \rho) d^3 r'_1.$$

Using Eqs. (21) and (10), the second-order dipole energy may be written as

$$\begin{aligned} E_{\kappa=1}^{[2]}(X\nu R n L N) = e^2 \sum_{\alpha\Lambda(\neq X), \nu', R', n', L'} \begin{Bmatrix} R' & L' & N \\ R & L & 1 \end{Bmatrix}^2 (2L+1)(2L'+1) \begin{Bmatrix} L & 1 & L' \\ 0 & 0 & 0 \end{Bmatrix}^2 (2R+1)(2R'+1) \\ \times \begin{Bmatrix} R & 1 & R' \\ 0 & -\Lambda & \Lambda \end{Bmatrix}^2 \left[\int g_{X\nu R}(\rho) D_{X,\alpha\Lambda}(\rho) g_{\alpha\Lambda\nu'R'}(\rho) d\rho \right]^2 \\ \times \left[\frac{[nL \| r_2^{-2} \| n' L']^2}{E^0(X\nu R) - E^0(\alpha\Lambda\nu'R')} - \frac{[E^0(n) - E^0(n')][nL \| r_2^{-2} \| n' L']^2}{[E^0(X\nu R) - E^0(\alpha\Lambda\nu'R')]^2} + \dots \right]. \end{aligned} \quad (23)$$

The sum over n' , in both adiabatic and nonadiabatic terms, can be evaluated exactly using the properties of the hydrogenic radial eigenfunctions. The completeness of radial functions of fixed L' implies

$$\sum_{n'} P_{n'L'}(x) P_{n'L'}(x') = \delta(x - x'), \quad (24)$$

from which

$$\sum_{n'} [nL \| r_2^{-2} \| n' L']^2 = [nL \| r_2^{-4} \| nL]. \quad (25)$$

From the fact that the radial functions satisfy

$$\frac{1}{n^2} P_{nL}(r) = a_0^2 \left[\frac{d^2}{dr^2} + \frac{2}{a_0 r} - \frac{L(L+1)}{r^2} \right] P_{nL}(r),$$

it can be shown, using integration by parts, that for $L \geq 2$,

$$\sum_{n'} [E^0(n) - E^0(n')][nL \| r_2^{-2} \| n' L']^2 = \frac{e^2 a_0}{2} [L(L+1) - L'(L'+1) - 4][nL \| r_2^{-6} \| nL]. \quad (26)$$

Following Brieger,¹⁸ we introduce definitions of the electronic branch polarizabilities,

$$\alpha_{\parallel}^{X\nu}(R, R') \equiv -2 \sum_{\alpha, \nu'} \frac{\left[\int g_{X\nu R}(\rho) D_{X,\alpha\Lambda=0}(\rho) g_{\alpha\Lambda=0\nu'R'}(\rho) d\rho \right]^2}{E^0(X\nu R) - E^0(\alpha\Lambda=0\nu'R')}, \quad (27a)$$

and

$$\alpha_{\perp}^{X\nu}(R, R') \equiv -2 \sum_{\alpha, \nu'} \frac{\left[\int g_{X\nu R}(\rho) D_{X, \alpha \Lambda=1}(\rho) g_{\alpha \Lambda=1 \nu' R'}(\rho) d\rho \right]^2}{E^0(X\nu R) - E^0(\alpha \Lambda=1 \nu' R')}, \quad (27b)$$

and, by analogy, define the nonadiabatic coefficients

$$\beta_{\parallel}^{X\nu}(R, R') \equiv 2 \sum_{\alpha, \nu'} \frac{\left[\int g_{X\nu R}(\rho) D_{X, \alpha \Lambda=0}(\rho) g_{\alpha \Lambda=0 \nu' R'}(\rho) d\rho \right]^2}{[E^0(X\nu R) - E^0(\alpha \Lambda=0 \nu' R')]^2}, \quad (28a)$$

and

$$\beta_{\perp}^{X\nu}(R, R') \equiv 2 \sum_{\alpha, \nu'} \frac{\left[\int g_{X\nu R}(\rho) D_{X, \alpha \Lambda=1}(\rho) g_{\alpha \Lambda=1 \nu' R'}(\rho) d\rho \right]^2}{[E^0(X\nu R) - E^0(\alpha \Lambda=1 \nu' R')]^2}, \quad (28b)$$

with which the second-order dipole energy may be written as

$$\begin{aligned} E_{\kappa=1}^{[2]}(X\nu R n L N) = & -\frac{e^2}{2} [nL \| r^{-4} \| nL] \sum_{R', L'} \left\{ \begin{matrix} R' & L' & N \\ L & R & 1 \end{matrix} \right\}^2 (2L+1)(2L'+1) \left[\begin{matrix} L & 1 & L' \\ 0 & 0 & 0 \end{matrix} \right]^2 \\ & \times (2R+1)(2R'+1) \left[\left[\begin{matrix} R & 1 & R' \\ 0 & 0 & 0 \end{matrix} \right]^2 \alpha_{\parallel}^{X\nu}(R, R') + 2 \left[\begin{matrix} R & 1 & R' \\ 0 & -1 & 1 \end{matrix} \right]^2 \alpha_{\perp}^{X\nu}(R, R') \right] \\ & - \frac{e^4 a_0}{4} [nL \| r^{-6} \| nL] \sum_{R', L'} \left\{ \begin{matrix} R' & L' & N \\ L & R & 1 \end{matrix} \right\}^2 (2L+1)(2L'+1) \left[\begin{matrix} L & 1 & L' \\ 0 & 0 & 0 \end{matrix} \right]^2 \\ & \times (2R+1)(2R'+1) \left[\left[\begin{matrix} R & 1 & R' \\ 0 & 0 & 0 \end{matrix} \right]^2 \beta_{\parallel}^{X\nu}(R, R') \right. \\ & \quad \left. + 2 \left[\begin{matrix} R & 1 & R' \\ 0 & -1 & 1 \end{matrix} \right]^2 \beta_{\perp}^{X\nu}(R, R') \right] \\ & \times [L(L+1) - L'(L'+1) - 4] + \dots \end{aligned} \quad (29)$$

To simplify further, it is necessary to note that while the coefficients $\alpha(R, R')$ and $\beta(R, R')$ do depend on R' , the dependence is a weak one arising from the centrifugal distortion of the vibrational wave functions $g(\rho)$ and the rotational energies implied in the denominators of Eqs. (27) and (28).

Again following Brieger,¹⁸ we introduce the definition of the branch average polarizabilities and nonadiabatic coefficients and, for the present, neglect the differences between the individual rotational branches and the average. This gives

$$\alpha_{\parallel}^{X\nu}(R, R') \cong \frac{1}{2} [\alpha_{\parallel}^{X\nu}(R, R+1) + \alpha_{\parallel}^{X\nu}(R, R-1)] \equiv \alpha_{\parallel}^{X\nu}(R), \quad (30a)$$

and

$$\begin{aligned} \alpha_{\perp}^{X\nu}(R, R') & \cong \frac{1}{3} [\alpha_{\perp}^{X\nu}(R, R+1) + \alpha_{\perp}^{X\nu}(R, R) + \alpha_{\perp}^{X\nu}(R, R-1)] \\ & \equiv \alpha_{\perp}^{X\nu}(R), \end{aligned} \quad (30b)$$

and similarly,

$$\begin{aligned} \beta_{\parallel}^{X\nu}(R, R') & \cong \frac{1}{2} [\beta_{\parallel}^{X\nu}(R, R+1) + \beta_{\parallel}^{X\nu}(R, R-1)] \\ & \equiv \beta_{\parallel}^{X\nu}(R), \end{aligned} \quad (31a)$$

and

$$\begin{aligned} \beta_{\perp}^{X\nu}(R, R') & \cong \frac{1}{3} [\beta_{\perp}^{X\nu}(R, R+1) + \beta_{\perp}^{X\nu}(R, R) + \beta_{\perp}^{X\nu}(R, R-1)] \\ & \equiv \beta_{\perp}^{X\nu}(R). \end{aligned} \quad (31b)$$

With this approximation, Eq. (29) contains factors such as

$$\left[\begin{matrix} R & 1 & R' \\ 0 & 0 & 0 \end{matrix} \right]^2 \alpha_{\parallel}^{X\nu}(R) + 2 \left[\begin{matrix} R & 1 & R' \\ 0 & -1 & 1 \end{matrix} \right]^2 \alpha_{\perp}^{X\nu}(R) = \alpha_s^{X\nu}(R) \frac{1}{(2R+1)} + \alpha_T^{X\nu}(R) \left[\left[\begin{matrix} R & 1 & R' \\ 0 & 0 & 0 \end{matrix} \right]^2 - \frac{1}{3(2R+1)} \right],$$

where

$$\alpha_s^{X\nu}(R) \equiv \frac{1}{3} [\alpha_{\parallel}^{X\nu}(R) + 2\alpha_{\perp}^{X\nu}(R)], \quad \alpha_T^{X\nu}(R) \equiv \alpha_{\parallel}^{X\nu}(R) - \alpha_{\perp}^{X\nu}(R). \quad (32)$$

Similar terms occur for β and can be written in terms of

$$\beta_s^{X\nu}(R) \equiv \frac{1}{3}[\beta_{\parallel}^{X\nu}(R) + 2\beta_{\perp}^{X\nu}(R)], \quad \beta_T^{X\nu}(R) \equiv \beta_{\parallel}^{X\nu}(R) - \beta_{\perp}^{X\nu}(R). \quad (33)$$

The sums over R' and L' in Eq. (29) may be evaluated with the results

$$\sum_{R',L'} \begin{Bmatrix} R' & L' & N \\ L & R & 1 \end{Bmatrix}^2 (2R'+1)(2L+1)(2L'+1) \begin{Bmatrix} L & 1 & L' \\ 0 & 0 & 0 \end{Bmatrix}^2 = 1, \quad (34a)$$

$$\begin{aligned} \sum_{R',L'} \begin{Bmatrix} R' & L' & N \\ L & R & 1 \end{Bmatrix}^2 (2R+1)(2R'+1)(2L+1)(2L'+1) \begin{Bmatrix} L & 1 & L' \\ 0 & 0 & 0 \end{Bmatrix}^2 \left[\begin{Bmatrix} R & 1 & R' \\ 0 & 0 & 0 \end{Bmatrix}^2 - \frac{1}{3(2R+1)} \right] \\ = \frac{2}{3} \left[\frac{3S(S-1) - 4L(L+1)R(R+1)}{2(2R-1)(2R+3)(2L-1)(2L+3)} \right] = \frac{2}{3} \langle RLN | P_2(\cos\theta) | RLN \rangle, \quad (34b) \end{aligned}$$

where $S = R(R+1) + L(L+1) - N(N+1)$ and where the last form of Eq. (34b) identifies the expression in the previous parentheses as the expectation value of $P_2(\cos\theta_{2\hat{p}})$ in vector-coupled spherical harmonic eigenstates of R and L . Similarly, one can show that

$$\sum_{R',L'} \begin{Bmatrix} R' & L' & N \\ L & R & 1 \end{Bmatrix}^2 (2R'+1)(2L+1)(2L'+1) \begin{Bmatrix} L & 1 & L' \\ 0 & 0 & 0 \end{Bmatrix}^2 [L(L+1) - L'(L'+1) - 4] = -6 \quad (34c)$$

and

$$\begin{aligned} \sum_{R',L'} \begin{Bmatrix} R' & L' & N \\ L & R & 1 \end{Bmatrix}^2 (2R+1)(2R'+1)(2L+1)(2L'+1) \begin{Bmatrix} L & 1 & L' \\ 0 & 0 & 0 \end{Bmatrix}^2 [L(L+1) - L'(L'+1) - 4] \\ \times \left[\begin{Bmatrix} R & 1 & R' \\ 0 & 0 & 0 \end{Bmatrix}^2 - \frac{1}{3(2R+1)} \right] = -2 \langle RLN | P_2(\cos\theta) | RLN \rangle. \quad (34d) \end{aligned}$$

Combining these results, the final expression for the dipole polarization energy is

$$\begin{aligned} E_{\kappa=1}^{[2]}(X\nu RnLN) = -\frac{e^2}{2} \alpha_s^{X\nu}(R) [nL \| r^{-4} \| nL] - \frac{e^2}{3} \alpha_T^{X\nu}(R) [nL \| r^{-4} \| nL] \langle RLN | P_2(\cos\theta) | RLN \rangle \\ + \frac{3}{2} e^4 a_0 \beta_s^{X\nu}(R) [nL \| r^{-6} \| nL] + \frac{1}{2} e^4 a_0 \beta_T^{X\nu}(R) [nL \| r^{-6} \| nL] \langle RLN | P_2(\cos\theta) | RLN \rangle + \dots \quad (35) \end{aligned}$$

The coefficients $\alpha_s^{X\nu}(R)$ and $\alpha_T^{X\nu}(R)$, which occur in Eq. (35) and are defined by Eqs. (27) and (32), may be expected to be approximately equal to the vibrationally averaged scalar and tensor polarizabilities calculated by Bishop and Lam.¹⁹ The connection is only approximate since the calculations of electronic polarizability were carried out for a number of fixed internuclear separations and then averaged over the appropriate rovibrational wave functions. The near equivalence of this approach to the polarizabilities specified in Eqs. (27) and (32) is discussed by Schulman *et al.*²⁰, who conclude that errors on the order of 10^{-3} in the polarizabilities may be expected in this method of calculation. This is probably the same degree of approximation which is incurred by neglecting differences in the branch polarizabilities in Eqs. (30) and (31).

With the same reservations regarding the manner of inclusion of the nuclear motion, the parameters $\beta_s^{X\nu}(R)$ and $\beta_T^{X\nu}(R)$ occurring in Eq. (35) and defined by Eqs. (28) and (33) are expected to be approximately equal to the "moment functions" S_{-3} defined and tabulated by Bishop and Cheung.²¹

Summarizing to this point, a systematic perturbation-

theory treatment of the Rydberg state energy indicates, in addition to the zeroth-order energy, contributions from (a) the first-order perturbation energies due to the static multiple moments of H_2^+ , which are given by Eq. (15); (b) the polarization energies due to the portion of the second-order perturbation energy off-diagonal in the core electronic state, which are given (in the case of $\kappa=1$) by Eq. (35); and (c) the interseries perturbation energies due to the static multipole potential (that is, the portion of the second-order energy that is diagonal in core electronic state), which is given by Eq. (20). The first two of these effects may be approximated as the expectation value of a polarization potential, of which Eq. (1) (LOPM) gives the leading terms. Higher-order terms are generally proportional to a higher inverse power of r_2 and so give smaller contributions, especially for high- L states. The effects of (c) have, in the past, been estimated by using Eq. (1) to couple different Rydberg series.^{1,3,5,17} This approach appears questionable in view of the different origin of the static quadrupole and polarization terms in Eq. (1). To second order in perturbation theory, only the static multipole potential produces interseries mixing. Mixing due to the dipole polarization potential,

if it occurs, would be included in a systematic treatment of higher-order perturbation terms, and whether the simple usage of the potential of Eq. (1) would be justified is an open question.

As expected, the dipole polarization energy is approximately equal to the energy of the H_2^+ ion in the electric field produced by a stationary Rydberg electron. There are, however, significant "nonadiabatic" corrections to this picture which lead to additional contributions to the polarization potential, typically opposite in sign and proportional to a higher inverse power of r_2 . As in the atomic case,²² these nonadiabatic terms may also be parametrized in terms of coefficients which are properties of the free-core ion.

Another conclusion which can be drawn from the calculation in the preceding is that when the rotation of the core is properly included, the adiabatic dipole polarization energies are not strictly parametrized by two coefficients (α_s, α_T), but rather by a larger number (typically five) of parameters which we refer to as electronic branch polarizabilities [Eq. (27)]. The reduction to the two-parameter form is an approximation. Similarly, it is an approximation to write the polarizability as an average, over core vibrational wave functions, of the polarizability at fixed internuclear separation. These conclusions are not unique to the application to Rydberg states, but are similar to the conclusions reached by others^{18,20} in studying the polarization energies of free diatomic molecules. Finally, it should be emphasized that in the calculation in the preceding, it has been assumed that the core wave functions could be written in the Born-Oppenheimer form [Eq. (6)] for both ground and excited states of the core, and that corrections to this picture could be ignored.

A. Higher-order extensions of the polarization model

A further extension of the polarization model, analogous to the treatment of helium by Drachman,¹¹ would

$$E = E^0 - \frac{e^2}{2} \alpha_s r^{-4} - \frac{e^2}{3} \alpha_T r^{-4} P_2(\cos\theta) - \frac{e^2}{10} C_0 r^{-6} - \frac{e^2}{7} C_1 r^{-6} P_2(\cos\theta) - \frac{12e^2}{35} C_2 r^{-6} P_4(\cos\theta) - \frac{e^3}{15} B_0 r^{-7} - \frac{e^3}{42} B_1 r^{-7} P_2(\cos\theta) - \frac{2e^3}{35} B_2 r^{-7} P_4(\cos\theta) - \frac{e^4}{24} \gamma_0 r^{-8} - \frac{e^4}{126} \gamma_1 r^{-8} P_2(\cos\theta) - \frac{e^4}{105} \gamma_2 r^{-8} P_4(\cos\theta), \quad (37)$$

where

$$\begin{aligned} \alpha_s &\equiv \frac{1}{3}(\alpha_{zz} + 2\alpha_{xx}), \\ \alpha_T &\equiv \alpha_{zz} - \alpha_{xx}, \\ C_0 &\equiv C_{zzzz} + 8C_{xzxz} + 8C_{xxxx}, \\ C_1 &\equiv 5C_{zzzz} + 4C_{xzxz} - 8C_{xxxx}, \\ C_2 &\equiv 2C_{zzzz} - 4C_{xzxz} + C_{xxxx}, \\ B_0 &\equiv B_{zzzz} + 4B_{xzxz} + B_{xxzz} + 4B_{xxxx}, \\ B_1 &\equiv 11B_{zzzz} + 8B_{xzxz} + 2B_{xxzz} - 16B_{xxxx}, \end{aligned}$$

calculate *all* terms in the polarization potential proportional to a given inverse power of r_2 through the systematic application of the following three separate expansions.

- (1) The Rayleigh-Schrödinger perturbation expansion of the state energy in powers of the perturbing potential V .
- (2) The multipole expansion of the potential V .
- (3) The expansion of energy denominators, analogous to Eq. (21).

Such a calculation is beyond the scope of this paper, but certain aspects of the result may be anticipated from existing calculations. Terms of zeroth order in the third expansion are the "adiabatic" terms which are expected to produce a result approximately equal to the energy of a polarizable H_2^+ ion in the electric field of a stationary Rydberg electron. Many of the consequences of such a field have already been calculated. In the notation of Buckingham,²³ the perturbed energy of such a system is

$$E = E^0 - \frac{1}{2} \alpha_{\alpha\beta} F_\alpha F_\beta - \frac{1}{24} \gamma_{\alpha\beta\gamma\delta} F_\alpha F_\beta F_\gamma F_\delta - \frac{1}{6} B_{\alpha\beta\gamma\delta} F_\alpha F_\beta F_\gamma F_\delta - \frac{1}{6} C_{\alpha\beta\gamma\delta} F_{\alpha\beta} F_{\gamma\delta} + \dots, \quad (36)$$

where α , γ , β , and C are Cartesian tensors giving the dipole polarizability (α), hyperpolarizability (γ), and quadrupole polarizabilities (B and C). The indices α , β , γ , and δ denote the Cartesian components x , y , and z . F_α is the electric field and $F_{\alpha\beta}$ the electric field gradient tensor. If we consider the electric field exerted on the H_2^+ ion by the Rydberg electron at a distance r and polar angle θ from the internuclear axis $\hat{\rho}$, and use the expressions of Buckingham for the polarizability tensor components for axially symmetric molecules, we find the expression

$$B_2 \equiv 3B_{zzzz} - 8B_{xzxz} - 2B_{xxzz} + 2B_{xxxx},$$

$$\gamma_0 \equiv \frac{1}{15}(8\gamma_{xxxx} + 3\gamma_{zzzz} + 12\gamma_{xzxz}),$$

$$\gamma_1 \equiv 3\gamma_{zzzz} - 4\gamma_{xxxx} + 3\gamma_{xzxz},$$

$$\gamma_2 \equiv \gamma_{zzzz} + \gamma_{xxxx} - 6\gamma_{xzxz},$$

and in each case the Cartesian components of the polarizability tensors are defined in the frame whose z axis is along the internuclear axis $\hat{\rho}$. All of the relevant polarizability components needed to evaluate Eq. (37) in the case of H_2^+ have been calculated by Bishop and Lam.¹⁹

One additional adiabatic polarization term, which also

gives a contribution proportional to r_2^{-6} but which is not included in the expressions of Buckingham, is the dipole-octupole polarization energy.^{24,25} This is expressed in terms of a tensor $E_{\alpha\beta\gamma\delta}$ having two independent components for an axially symmetric molecule, and gives a contribution to the energy which can be written as²⁵

$$\Delta E = -\frac{1}{6}[-2E_{x:xxx}(F_x F_{xzz} + F_y F_{yzz}) + E_{z:zzz} F_z F_{zzz}],$$

where

$$F_{xzz} = \frac{\partial^2}{\partial z^2} F_x, \dots$$

Again, substituting the electric field of the Rydberg electron, this reduces to the form

$$\Delta E = -\frac{1}{7}E_1 P_2(\cos\theta)e^2/r_2^6 - \frac{1}{35}E_2 P_4(\cos\theta)e^2/r_2^6, \quad (38)$$

with

$$E_1 = 3E_{z:zzz} - 8E_{x:xxx}, \quad E_2 = 4E_{z:zzz} + 8E_{x:xxx}.$$

The E tensor has been calculated for HF by Bishop and Maroulis.²⁴ The first calculations of the E tensor for H_2^+ have been carried out recently.²⁶

All of these terms would be expected to contribute to the adiabatic portion of the polarization potential in an extended calculation. In addition, nonadiabatic corrections to each term would produce other contributions to the potential, proportional to higher inverse powers of r_2 . Ignoring, for the moment, the effects of interseries mixing [Eq. (20)], the energy of a particular Rydberg state in the polarization model is given by the expectation value of this series. For Rydberg states built on $R=0$ cores, only isotropic terms contribute, giving a structure which is very similar to the helium atom. For states built on $R=1$ cores, such as those reported here, terms proportional to $P_2(\cos\theta)$ also contribute, giving a structure of the form

$$E((\nu, 1)nL_n) = E^0(\nu, 1, n) + A_0(\nu, 1, n, L) + A_2(\nu, 1, n, L) \langle RLN | P_2(\cos\theta) | RLN \rangle,$$

where $\langle RLN | P_2(\cos\theta) | RLN \rangle$ is given in Eq. (34b).

The scalar (A_0) and tensor (A_2) structure factors form a convenient parametrization of the structure which facilitates comparison with experiment. Each can be expressed as the expectation value of a series of terms proportional to increasing negative powers of r_2 . Using the results derived in the preceding, we get

$$\begin{aligned} A_0(\nu, R, n, L) &= -\frac{e^2}{2}\alpha_S^{X\nu}(R)[nL \| r^{-4} \| nL] + \frac{1}{2}e^4 a_0 \beta_S^{X\nu}(R)[nL \| r^{-6} \| nL] - \frac{1}{10}e^2 C_0(\nu, R)[nL \| r^{-6} \| nL] \\ &\quad - \frac{1}{15}e^3 B_0(\nu, R)[nL \| r^{-7} \| nL] - \frac{1}{24}e^4 \gamma_0(\nu, R)[nL \| r^{-8} \| nL] + \dots, \\ A_2(\nu, R, n, L) &= -eQ(\nu, R)[nL \| r^{-3} \| nL] - \frac{e^2}{3}\alpha_T^{X\nu}(R)[nL \| r^{-4} \| nL] + \frac{1}{2}e^4 a \beta_T^{X\nu}(R)[nL \| r^{-6} \| nL] \\ &\quad - \frac{1}{7}e^2 C_1(\nu, R)[nL \| r^{-6} \| nL] - \frac{1}{7}e^2 E_1(\nu, R)[nL \| r^{-6} \| nL] - \frac{1}{42}e^3 B_1(\nu, R)[nL \| r^{-7} \| nL] \\ &\quad - \frac{1}{126}e^4 \gamma_1(\nu, R)[nL \| r^{-8} \| nL] + \dots. \end{aligned}$$

In order to evaluate these expressions, the relevant coefficients, for the $(\nu, R)=(0, 1)$ state of H_2^+ , are needed. For the quadrupole moment and dipolar polarizabilities, we use the recent results of Bishop and Lam,²⁷

$$Q(0, 1) = 1.64257ea_0^2,$$

$$\alpha_{zz}(0, 1) = 5.8657a_0^3,$$

$$\alpha_{xx}(0, 1) = 1.8384a_0^3,$$

giving

$$\alpha_S^{X0}(1) = 3.1809a_0^3, \quad \alpha_T^{X0}(1) = 4.0273a_0^3.$$

For the nonadiabatic dipole polarizability coefficients, we use the S_{-3} -moment functions calculated by Bishop and Cheung.²¹ Calculation of the tensor component and averaging over the appropriate vibrational wave function have been carried out by Bishop,²⁸ with the results

$$\beta_S^{X0}(1) = \frac{1}{3}[(S_{-3})_{\parallel} + 2(S_{-3})_{\perp}] = 6.8406a_0^4/e^2,$$

$$\beta_T^{X0}(1) = (S_{-3})_{\parallel} - (S_{-3})_{\perp} = 12.4906a_0^4/e^2.$$

The adiabatic quadrupole polarizabilities have been calculated by Bishop and Lam,²⁷ with the results

$$C_{zz,zz}(0, 1) = 10.09a_0^5,$$

$$C_{xz,xz}(0, 1) = 1.34a_0^5,$$

$$C_{xx,xx}(0, 1) = 3.37a_0^5,$$

from which we get

$$C_0(0, 1) = 47.77a_0^5, \quad C_1(0, 1) = 28.83a_0^5.$$

These polarizabilities are dominated by the vibrational contributions (i.e., by the tendency of the internuclear distance to change in the presence of an electric field gra-

dient).

For the dipole-dipole-quadrupole polarizabilities B and the hyperpolarizabilities γ , we again take the values from the calculations of Bishop and Lam,²⁷

$$\begin{aligned} B_{z,z,zz}(0,1) &= 82.72a_0^6/e, \\ B_{x,z,xz}(0,1) &= -21.91a_0^6/e, \\ B_{x,x,xz}(0,1) &= 26.49a_0^6/e, \\ B_{x,x,xx}(0,1) &= -23.93a_0^6/e, \\ \gamma_{zzzz}(0,1) &= 2222.42a_0^7/e^2, \\ \gamma_{xxzz}(0,1) &= 134.82a_0^7/e^2, \\ \gamma_{xxxx}(0,1) &= 126.04a_0^7/e^2, \end{aligned}$$

from which we get

$$\begin{aligned} B_0(0,1) &= -74.18a_0^6/e, \\ B_1(0,1) &= 1171a_0^6/e, \\ \gamma_0(0,1) &= 619.6a_0^7/e^2, \\ \gamma_1(0,1) &= 6568a_0^7/e^2. \end{aligned}$$

The E tensor coefficients calculated recently by Bishop²⁶ are

$$E_{z,zzz} = 5.901a_0^5, \quad E_{x,xxx} = 1.130a_0^5,$$

This gives

$$E_1 = 8.663a_0^5.$$

The expectation values of the several terms in the polarization potential may be evaluated using these coefficients and the expectation values of r^{-s} in hydrogenic wave functions tabulated by Bockasten.²⁹ The results for $10F$, $10G$, $10H$, and $10I$ states of H_2 are shown in Table I.

For the scalar structure constant, the leading term has $s = -4$ and the leading correction terms have $s = -6$. Two higher-order terms, $s = -7$ and -8 , are included in Table I, but since there are a number of uncalculated nonadiabatic terms which are expected to give contributions of this order also, these are best regarded only as an indication of the likely convergence of the series. Contributions from successive terms decrease with increasing powers of $1/r_2$ until some critical power, after which they increase once again. This critical power increases with increasing L . This behavior is similar to that found by Drachman in his study of helium Rydberg states with the polarization model.¹¹ In order to estimate the sum of this asymptotic series, Drachman suggests grouping the terms from each power of $1/r_2$, and estimating the sum as the partial sum up to but not including the smallest calculated term, plus one-half the smallest term, with an estimated error that is one-half the smallest term. Using this rule and the calculated terms proportional to r^{-4} and r^{-6} , we obtain an improved estimate of the scalar structure constant for these states,

$$A_0^{\text{HOPM}} = (V_4 + \frac{1}{2}V_6) \pm \frac{1}{2}V_6, \quad (39)$$

where V_s is the sum of all terms proportional to r_2^{-s} . This improved estimate is included in Table I, where it is labeled by HOPM (higher-order polarization model). Also shown for comparison is the prediction of the lowest order-model (LOPM). The principal advantage of the extended model is that it gives an indication of the probable precision of the prediction.

For the tensor constant A_2 , the leading term is the quadrupole term ($s = -3$), with additional contributions from $s = -4$ and -6 terms. Combining these terms, using the same procedure to estimate their sum, we obtain an improved estimate of the tensor constant A_2 ,

$$A_2^{\text{HOPM}} = (V_3 + V_4 + \frac{1}{2}V_6) \pm \frac{1}{2}V_6, \quad (40)$$

which is shown in Table I under the heading HOPM. Here the increase in precision with L is quite dramatic, reaching 15 ppm for the $10I$ state.

III. EXPERIMENT

The method used to study the spectroscopy of $n = 10$ Rydberg states of H_2 is the same as that described in Ref. 1. A beam of H_2^+ , of about 11 keV energy, is neutralized in a charge exchange cell. A portion of the fast neutral beam emerging from the cell is in the Rydberg states of interest, and can be sensitively detected by resonantly exciting those states with a laser to a very weakly bound state, such as $n = 27$, and then immediately Stark ionizing the upper state and collecting the resulting ions in a channel electron multiplier. The laser is a grating-tuned, fixed-frequency cw CO_2 laser (Advanced Kinetics MIRL-50), whose frequency is close enough to the desired transition frequency that fine tuning can be accomplished through the Doppler effect by varying the angle of intersection between the laser and the fast beam. The frequency resolution of the laser excitation spectrum, about 0.01 cm^{-1} , is determined by the angular spread in the beam and by transit and power broadening of the laser resonance. This gives sufficient resolution to show rather clearly the Rydberg fine structure in a study of the excitation spectrum. In Ref. 1, 19 different $n = 10$ Rydberg states were identified as contributing to the 10-27 excitation spectrum on the basis of their energies, which were shown to correspond to the predictions of the lowest-order polarization model to within the experimental precision of $\pm 0.02 - \pm 0.04 \text{ cm}^{-1}$.

For the present work, lines in the excitation spectrum corresponding to initial states $(0,1)10F_N$ and $(0,1)10G_N$ are studied more carefully. These states were chosen because their excitation spectra are complete and well resolved. In order to improve the precision of the optical spectroscopy, the Doppler-tuned laser frequency was checked by observing the 10-27 transition in atomic hydrogen with several different CO_2 laser lines, which match the excitation energy at a wide range of intersection angles. This also provides an improved determination of the beam energy. Figure 1 illustrates the construction of the Doppler-tuning stage, which is similar to

TABLE I. Calculated contributions to the scalar and tensor structure factors of (0,1) $10L$ states of H_2 with $3 \leq L \leq 6$. Numbers in parentheses denote errors.

$-s$	Coefficient	$A_0(0,1,10,L)$ (cm^{-1})			
		$10F$	$10G$	$10H$	$10I$
4	α_S	-1.0638	-0.282 07	-0.097 640	-0.039 986
6	β_S	0.2288	0.016 31	0.002 103	0.000 378
6	C_0	-0.1065	-0.007 59	-0.000 979	-0.000 176
7	B_0	0.0324	0.000 97	0.000 071	0.000 008
8	γ_0	-0.0938	-0.000 79	-0.000 030	-0.000 002
			LOPM		
		-1.0638	-0.2821	-0.097 640	-0.039 986
			HOPM		
		-1.003(61)	-0.2777(44)	-0.097 08(56)	-0.039 89(10)
			$A_2(0,1,10,L)$ (cm^{-1})		
3	Q	-8.5834	-4.0056	-2.184 87	-1.320 52
4	α_T	-0.8979	-0.2381	-0.082 41	-0.033 75
6	β_T	0.1393	0.0099	0.001 28	0.000 23
6	C_1	-0.0918	-0.0065	-0.000 84	-0.000 15
6	E_1	-0.0276	-0.0020	-0.000 25	-0.000 04
7	B_1	-0.1824	-0.0054	-0.000 40	-0.000 046
8	γ_1	-0.1895	-0.0016	-0.000 06	-0.000 004
			LOPM		
		-9.4813	-4.2437	-2.267 28	-1.354 27
			HOPM		
		-9.471(10)	-4.2430(7)	-2.267 19(9)	-1.354 26(2)

that used by Kugel *et al.*³⁰ The CO_2 laser enters the high-vacuum chamber approximately along the rotation axis of the stage and is directed to an intersection with the fast beam, also approximately on the rotation axis, by two plane mirrors. The rotational motion of the stage is computer controlled through a precision rotation stage

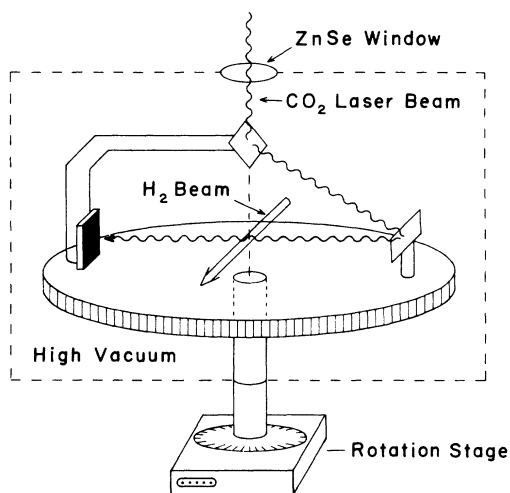


FIG. 1. Doppler-tuning stage. The CO_2 laser enters and intersects the fast H_2 beam on the rotation axis of the stage. Rotary motion is computer controlled through a precision rotation stage.

(Newport model 499 with 855 controller). With an ideal alignment of the incident laser beam, the relative intersection angle can be read directly from the rotation stage. The incident laser beam alignment is monitored frequently and may be adjusted using removable pinholes, mounted externally to the vacuum chamber, and a tracer helium-neon laser beam. The rotary stage is initially mounted so that a reading of 0° corresponds roughly with antiparallel propagation of laser and fast beams.

Table II summarizes the observed angular positions of 10-27 transitions in atomic hydrogen observed with several CO_2 laser lines. The atomic hydrogen was obtained from protons of nominal energy 10.98 keV, as measured with a voltage divider (Data Precision model V41-A). The first two columns of Table II identify the laser line and give its known frequency.³¹ Since the laser was not stabilized to the center of the gain profile, its actual frequency is expected to vary by about ± 0.001 cm^{-1} due to frequency drift within the 0.003 - cm^{-1} gain profile. The free spectral range of the laser is 0.003 cm^{-1} , so that at most two longitudinal modes were likely to be active. The laser operated in a pure TEM_{00} transverse mode. The calculated frequency for the 10-27 excitation in atomic hydrogen is 946.327 cm^{-1} . The third column of Table II gives the observed angular positions of this resonance with the several laser lines, as determined from line profiles plotted against the angular readout of the stage controller. Measurement error is less than 0.01° . All of these observations could be accounted for with the Doppler-tuning formula

TABLE II. Calibration measurements for Doppler-tuned laser frequency. Numbers in parentheses denote errors.

CO ₂ line	Transition is H(10-27) at 946.327 cm ⁻¹		
	ν_L (cm ⁻¹)	θ^{obs} (deg)	θ^{fit} (deg)
P(14)	949.479	-134.04	-133.97
P(16)	947.742	-108.18	-108.22
P(18)	945.980	-85.41	-85.48
P(20)	944.194	-61.59	-61.62
P(22)	942.383	-29.64	-29.56
P(22)	942.383	32.18	32.26
P(20)	944.194	63.32	63.20
P(18)	945.980	85.98	85.94
P(16)	949.742	107.52	107.60
P(14)	949.479	132.30	132.28

Fit results: $\theta = \theta^{\text{obs}} + A + B \cos\theta + C \sin\theta$
 $A = 0.139(29)^\circ$, $B = 1.421(51)^\circ$, $C = -0.101(34)^\circ$, $\beta = 0.0048669(27)$

$$\nu' = \frac{\nu_L [1 + \beta \cos(\theta)]}{\sqrt{1 - \beta^2}} \quad (41)$$

if θ , the actual intersection angle, is given in terms of the angle measured by the rotation stage, θ_{stage} , by

$$\theta = \theta_{\text{stage}} + A + B \cos(\theta) + C \sin(\theta). \quad (42)$$

The offset angle A reflects the initial rough setting of $\theta_{\text{stage}} = 0$, while the sinusoidal error is partially due to a misalignment of the incident CO₂ beam, which leads to “walking” of the laser on the internal mirrors as the stage turns, and partially due to a sinusoidal error in the angular readout from the rotation stage. Column 4 of Table II shows the best fit of the observed positions (column 3) using Eqs. (41) and (42) and varying β , A , B , and C . The rms deviation from the fit (0.07°) may be taken as a measure of the precision of the alignment procedure, since each observation required independent alignment of the laser with respect to the stage axis.

The value of β obtained from this fit was used to improve the calibration of the voltage divider measuring the beam energy, resulting in a calibration factor of 1.0124 ± 0.0013 , which is consistent with the expected 2% precision of this component. Using Eqs. (41) and (42), the frequency difference of two lines observed at $\theta(1)^{\text{obs}}$ and $\theta(2)^{\text{obs}}$, with the same choice of laser lines, could be inferred with somewhat higher precision than the absolute frequency of either. For this calculation, it was assumed that the angles $\theta(1)$ and $\theta(2)$ were given by Eq. (42), with the calibration constants given by

$$A = 0.130(92)^\circ, \quad B = 1.421(161)^\circ, \quad C = -0.101(108)^\circ.$$

The larger errors reflect the uncertainty associated with a *single* alignment of the laser.

Figure 2 illustrates the fine structure of a few $n = 10$ and 27 Rydberg states of H₂, showing the transitions studied here. Each of the three (0,1)10F_N states give rise to a single strong transition, labeled in Fig. 2 by capital letters A_i. Several weaker lines which correspond to

different final states are labeled by lower-case letters a_i. A similar labeling scheme is used for the lines with lower states (0,1)10G_N. Representative excitation spectra showing these lines are illustrated in Fig. 3. The angular positions of each of these lines, and comparable lines with final states in the $n = 26$ manifold, were measured. Table III summarizes the observed positions of the strongest lines. Also included is the position of the 10-26 (or 27) transition in atomic hydrogen, labeled H, observed in atoms produced by dissociation of H₂⁺ in the charge exchange cell. Since the frequency of this transition is known, the relative angular positions of the H₂ lines with

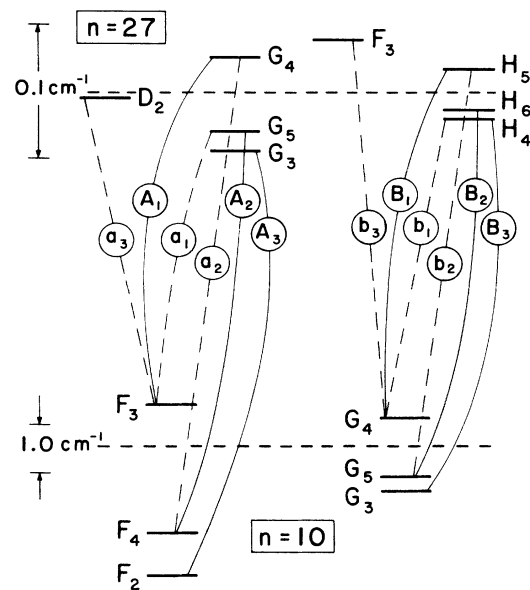


FIG. 2. Level diagram showing the electric fine structure (EFS) of $n = 10$ and $n = 27$ Rydberg states of H₂, and illustrating the optical transitions studied here.

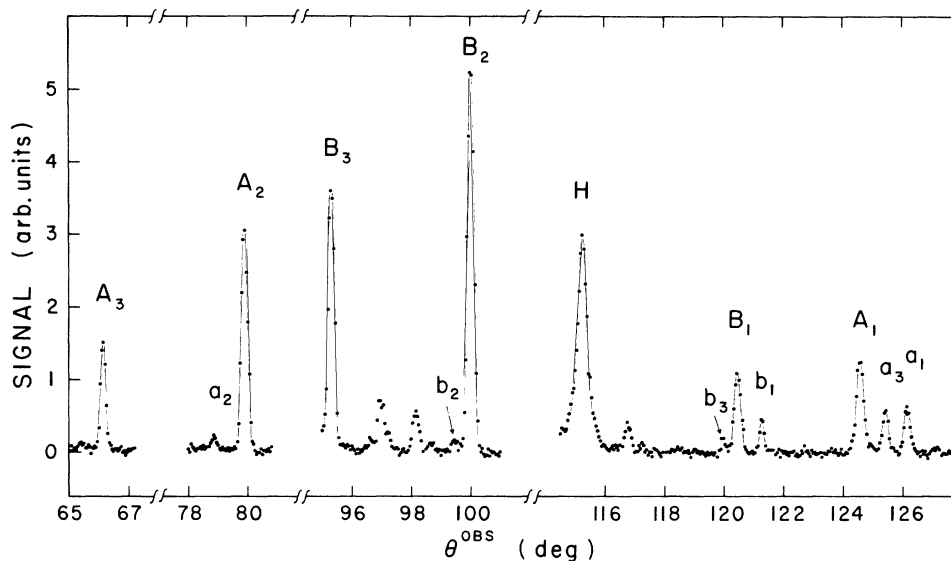


FIG. 3. Typical excitation spectrum of Doppler-tuned 10-27 Rydberg transitions in H_2 , using the $P(16)$ line of the CO_2 laser (947.742 cm^{-1}). The vertical axis is proportional to the number of ions per second entering the channel electron multiplier. The horizontal axis is the intersection angle between fast H_2 beam and the laser, as measured with the rotation stage.

respect to this line determine their energies with slightly higher precision than direct use of Eqs. (41) and (42). The intersection angles, shown in column 4 of Table III, were inferred from the observed line positions using the angular calibration constants discussed in the preceding. Those shown in column 5 were obtained from measurements of the relative angles, using the known frequency

of the hydrogenic transition H . The transition energies, shown in column 6, were determined from Eq. (41) with the beam velocity taken to be $\beta=0.0034409(21)$, as determined from the calibration of the beam energy discussed in the preceding. The last column of Table III shows the deviation of the transition energy from the zeroth-order hydrogenic value. These measurements, for

TABLE III. Measured frequencies of primary transitions in the excitation spectrum of $(0,1)10F$ and $(0,1)10G$ states of H_2 . Line identifications refer to Fig. 2. Numbers in parentheses denote errors.

Run	Line	θ^{obs} (deg)	θ (deg)	θ' (deg)	ν_0 (cm^{-1})	Δ (cm^{-1})
10-26 transitions, using $P(30)$ at 934.894 cm^{-1}						
1	A_3	42.537(5)	41.41(20)	41.38(20)	937.314(8)	2.529(8)
1	A_2	60.040(3)	59.27(17)			
2	A_2	60.129(4)	59.36(17)	59.24(13)	936.546(6)	1.761(6)
2	B_3	77.211(3)	76.86(15)	77.73(7)	935.638(4)	0.853(4)
2	B_2	82.003(2)	81.77(14)			
3	B_2	82.087(2)	81.86(14)	81.65(5)	935.367(3)	0.582(3)
3	H	96.656(2)	96.79(14)	96.59(17)	934.531 ^a	
3	B_1	101.381(4)	101.64(15)	101.43(2)	934.262(1)	-0.523(2)
3	A_1	104.868(3)	105.21(15)	105.00(3)	934.067(2)	-0.718(2)
10-27 transitions, using $P(16)$ at 947.742 cm^{-1}						
4	A_3	66.139(2)	65.51(16)	65.55(17)	949.098(9)	2.514(9)
4	A_2	79.891(2)	79.60(15)	79.64(13)	948.335(7)	1.751(7)
4	B_3	95.274(2)	95.38(14)			
5	B_3	95.317(2)	95.42(14)	95.42(7)	947.440(4)	0.856(4)
5	B_2	100.019(1)	100.24(15)	100.24(6)	947.168(3)	0.584(3)
5	H	115.254(4)	115.83(16)	115.83(3)	946.327 ^a	
6	H	115.248(4)	115.83(16)	115.83(3)	946.327 ^a	
6	B_1	120.462(3)	121.15(17)	121.15(3)	946.061(2)	-0.523(2)
6	A_1	124.573(3)	125.35(17)	124.35(4)	946.861(2)	-0.723(2)

^aCalculated value.

$n = 27$ upper states, can be compared directly with the less precise determinations of Ref. 1.

A possible systematic uncertainty in these measurements arises from the presence of electric fields in the region of laser excitation. Helmholtz coils were used to cancel the earth's magnetic field to reduce motional fields. Other fields, presumably due to charging of nominally conducting surfaces on the Doppler-tuning stage, were sometimes present, but could be reduced by careful collimation of the beam. In order to set experimental limits on the actual electric field present in the interaction region, a study of the effects of such fields on the $(0,1)10F_4$ - $(0,1)27G_5$ transition was made. In the rather large motional electric field which is present when the current in the Helmholtz coil is turned off (0.25 V/cm), this resonance was substantially altered, as shown in Fig. 4(a). The prominent feature at 948.35 cm^{-1} is the Stark-induced $(0,1)10F_4$ - $(0,1)27H_6$ transition which becomes allowed due to Stark mixing of the $(0,1)27G_5$ and $(0,1)27H_6$ states. The relative size of this feature and the dominant peak, in Fig. 4(a), is consistent with simulations based on

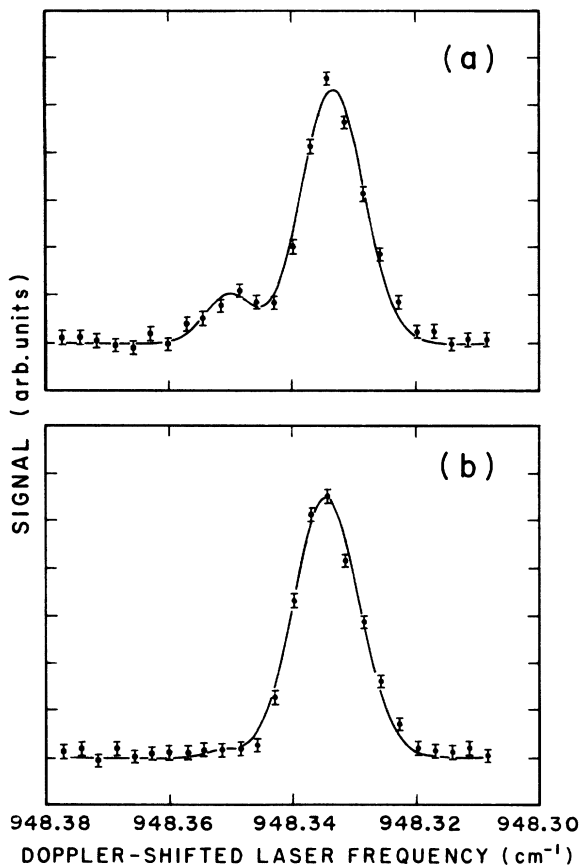


FIG. 4. $(0,1)10F_4$ - $(0,1)27G_5$ transition as it appears in the presence of a motional electric field of 0.25 V/cm (a) and under normal operating conditions (b). The feature of 948.35 in (a) is the Stark-induced $(0,1)10F_4$ - $(0,1)27H_6$ transition whose strength in (b) is used to estimate stray electric fields present in the region of interaction between the H_2 beam and the CO_2 laser.

the known electric dipole matrix elements connecting these states, their calculated zero-field separation (0.017 cm^{-1}), and an electric field of magnitude 0.25 V/cm. In the same region of the spectrum, observed under normal experimental conditions, as shown in Fig. 4(b), very little sign of this Stark-induced feature is evident, indicating an ambient electric field which is much less than 0.25 V/cm. More precise limits may be derived by fitting the spectrum to extract the size of the (very small) feature at the position where the Stark-induced feature is expected. By comparison with simulations, this gives an estimate of the ambient electric field. This test was repeated periodically during the period that data were taken for this experiment. Within the precision of these determinations, no significant changes with time were observed and the average field was estimated to be $0.06 \pm 0.10 \text{ V/cm}$. At this field strength, Stark shifts were negligible ($\leq 0.001 \text{ cm}^{-1}$), both for the upper and lower states of the transitions shown in Table III.

The positions of the six $n = 10$ Rydberg levels under study can be inferred from the measured excitation energies, using calculated values of the upper state EFS. As a check on this procedure, frequencies of the weaker lines shown in Figs. 2 and 3, relative to the primary lines, were determined and compared with the predictions of the LOPM. The results of this study, shown in Table IV, indicate that the upper-state structure agrees with the predictions of this model to within $\pm 0.001 \text{ cm}^{-1}$, with the exception of the line terminating on the $(0,1)27D_2$ state. Since only upper states with $L \geq 4$ are involved in the primary transitions, this is taken to indicate satisfactory agreement between the upper-state structure and the LOPM.

Table V shows the calculations used to determine the $n = 10$ Rydberg-level positions, relative to their zeroth-order energy $E(0,1) = 1097.074 \text{ cm}^{-1}$. The deviations of the transition frequencies from their zeroth-order values, Δ , from Table III, are shown in column 2 for both $n = 26$ and 27 upper states. Column 3 shows the calculated upper-state EFS in the LOPM. Column 4 gives the inferred $n = 10$ state EFS from each measurement, with the average for each state shown in column 5.

IV. COMPARISON WITH THEORY

In order to compare the measured positions of the $(0,1)10F_N$ and $(0,1)10G_N$ states with theory, we recall first that, with the exception of the portion of the second-order energy represented by Eq. (20), i.e., that part due to mixing with different Rydberg series, the energy of each state is expected to be of the form

$$E((\nu, R)nL_n) = E^0(\nu, R, n) + A_0(\nu, R, n, L) + A_2(\nu, R, n, L) \langle R|L|P_2(\cos\theta)|R\rangle.$$

Before the observed energies can be fit to extract the two structure factors (A_0 and A_2), the energy shifts due to Eq. (20) must be calculated and subtracted. These energy shifts were estimated using only the leading order multipole term in V , the quadrupole term. In this approximation they are given by

TABLE IV. Determinations of upper-state EFS from lines in the 10-27 excitation spectrum having a common lower state. Line identifications refer to Fig. 2. Numbers in parentheses denote errors.

Line	θ^{obs} (deg)	$\Delta\theta$ (deg)	ΔE (cm^{-1})	ΔE^{LOPM} (cm^{-1})	Interval
A_1	124.573(3)				
a_1	126.153(5)	1.611(8)	-0.075(1)	-0.074	G_3-G_4
a_3	125.421(5)	0.865(7)	-0.040(1)	-0.032	D_2-G_2
A_2	79.891(1)				
a_2	78.843(47)	1.075(47)	0.060(3)	0.059	G_4-G_5
B_1	120.462(2)				
b_1	121.273(4)	0.828(6)	-0.040(1)	-0.039	H_4-H_5
b_3	119.987(9)	-0.485(10)	0.024(1)	0.023	F_3-H_5
B_2	100.019(1)				
b_2	99.474(35)	-0.559(35)	0.031(2)	0.032	H_5-H_6

$$\Delta E((0,1)10L_N) = \sum_{\nu', R', n', L'} \frac{|\langle \nu' R' n' L' N | eQ(\rho) P_2(\cos\theta)/r_2^3 | (0,1)10L_N \rangle|^2}{E^0(0,1,10) - E^0(\nu' R' n')}$$

This expression contains contributions from many different Rydberg series satisfying the selection rules $\Delta N=0$, $\Delta R=0, \pm 2$, and $\Delta L=0, \pm 2$. For each such series, the sum over n' implicitly includes both discrete and continuum hydrogenic states with a fixed value of L' . The contribution from discrete states was estimated by explicitly calculating the contribution from each $n' \leq 25$ and extrapolating to include states with $n' > 25$. The contribution from continuum states was calculated for a sufficient range of $E > 0$ that the integral over E could be estimated numerically. An independent check of the total shift was obtained by calculating the total shift from a particular series using differential equation methods.³² Table VI illustrates the results of such calculations for the (0,1) $10G_5$ state. In most cases, the total contribution from a particular perturbing series is dominated by the contribution of the single state with an energy closest to

the level in question. For instance, 95% of the total shift of the (0,1) $10G_5$ state due to the (0,3) nG_5 series comes from mixing with the (0,3) $9G_5$ state.

Only the $\nu'=0, 1, 2$, and 3 , $R'=1, 3$ series were included in this estimate. The necessary matrix elements of $Q(\rho)$ were taken from the compilation of Bishop²⁷ to be

$$\begin{aligned} \langle 0,1 | Q(\rho) | 0,1 \rangle &= 1.6426ea_0^2, \\ \langle 0,3 | Q(\rho) | 0,3 \rangle &= 1.6618ea_0^2, \\ \langle 0,1 | Q(\rho) | 1,1 \rangle &= 0.3431ea_0^2, \\ \langle 0,3 | Q(\rho) | 1,3 \rangle &= 0.3460ea_0^2, \\ \langle 0,1 | Q(\rho) | 2,1 \rangle &= -0.0264ea_0^2, \\ \langle 0,3 | Q(\rho) | 2,3 \rangle &= -0.0267ea_0^2, \end{aligned}$$

TABLE V. Determination of $n=10$ EFS for (0,1) $10F$ and (0,1) $10G$ states from measured transition energies. All values in cm^{-1} . Numbers in parentheses denote errors.

Line	Δ (cm^{-1})	Upper-state EFS	$n=10$ EFS	Average	State
$A_3(26)$	2.529(8)	-0.052	-2.581(8)	-2.570(6)	(0,1) $10F_2$
$A_3(27)$	2.514(9)	-0.046	-2.560(9)		(0,1) $10F_2$
$A_2(26)$	1.761(6)	-0.035	-1.796(6)	-1.789(4)	(0,1) $10F_4$
$A_2(27)$	1.751(6)	-0.031	-1.782(6)		(0,1) $10F_4$
$A_1(26)$	-0.718(2)	0.031	0.749(2)	0.750(2)	(0,1) $10F_3$
$A_1(27)$	-0.723(2)	0.028	0.751(2)		(0,1) $10F_3$
$B_3(26)$	0.853(4)	-0.023	-0.876(4)	-0.876(3)	(0,1) $10G_3$
$B_3(27)$	0.856(4)	-0.021	-0.877(4)		(0,1) $10G_3$
$B_2(26)$	0.582(3)	-0.016	-0.598(3)	-0.598(2)	(0,1) $10G_5$
$B_2(27)$	0.584(3)	-0.014	-0.598(3)		(0,1) $10G_5$
$B_1(26)$	-0.523(2)	0.020	0.543(2)	0.542(2)	(0,1) $10G_4$
$B_1(27)$	-0.523(2)	0.018	0.541(2)		(0,1) $10G_4$

TABLE VI. Energy shifts of the (0,1)10G₅ state of H₂ due to (quadrupole) coupling to other Rydberg states. Values are in 10⁻⁴ cm⁻¹. The numbers in parentheses are uncertainties due to sensitivity to short-range ($r_2 < 2a_0$) contributions to the matrix elements of r_2^{-3} . Contributions from series with $\nu=2,3$ were also evaluated and were in all cases less than 10⁻⁵ cm⁻¹. Numbers in parentheses denote errors.

Series	$n' \leq 25$	$n' > 25$	$E > 0$	Total
(0,1)nG ₅	2.7	-0.5	-6.0	-3.8
(0,1)nI ₅	-0.1	0.0	-39.1	-39.2
(0,3)nD ₅	65.4(3)	0.0	-0.2	65.2(3)
(0,3)nG ₅	-238.7	-3.0	-39.4	-281.1
(0,3)nI ₅	0.0	0.0	-6.4	-6.4
(1,1)nG ₅	-0.5	0.0	-0.2	-0.7
(1,1)nI ₅	0.0	0.0	-1.4	-1.4
(1,3)nD ₅	3.5(1)	0.0	0.0	3.5(1)
(1,3)nG ₅	-1.9	0.0	-1.1	-3.0
(1,3)nI ₅	0.0	0.0	-0.2	-0.2
Total				-267.1(4)

$$\langle 0,1 | Q(\rho) | 3,1 \rangle = 0.0037ea_0^2,$$

$$\langle 0,3 | Q(\rho) | 3,3 \rangle = 0.0038ea_0^2.$$

Matrix elements of $Q(\rho)$ off-diagonal in core rotational quantum number R were approximated by the geometric mean of rotationally diagonal matrix elements. For instance,

$$\langle 0,1 | Q(\rho) | 1,3 \rangle \cong 0.3445ea_0^2.$$

Energy levels of the free H₂⁺ ion were taken from the compilation of Hunter *et al.*³³ In calculating the required integrals of r_2^{-3} between hydrogenic wave functions, the integrand was sufficiently small at small r_2 that the integral was relatively insensitive to the short-range behavior of the perturbing potential V [Eq. (5)], which is, of course, poorly approximated by the quadrupole term alone. In order to estimate the sensitivity of the result to short-range effects, the integrals were cut off at the minimum radius $r_{\min} = 2a_0$, and the result was considered uncertain by the difference from the full integral. This is the origin of the errors in the total calculated shift of each of the (0,1)10F and (0,1)10G states shown in Table VII. Note that the calculated shift is smaller for the

larger L state. This is to be expected since the positions of the perturbing levels are relatively constant with L but the coupling matrix elements decrease as L increases.

Using these calculated values of the contributions to the Rydberg-state energies from Eq. (20), the remainder can be fit to determine the structure parameters A_0 and A_2 for the (0,1)10F and (0,1)10G states. The results of this procedure are shown in Table VII. The fitted values of A_0 and A_2 given an excellent agreement with the observed structure. The estimated (1 standard deviation) errors in these parameters are derived from the errors shown in column 4 of Table VII, but *without* assuming that these errors are uncorrelated. This is necessary since they are derived from largely common systematic errors.

Table VIII compares the measured structure factors with the predictions of the polarization model (from Table I). For the scalar constants, measured and predicted values agree within the (6%) uncertainty of the theory for the 10F state, but the measured scalar constant for the 10G state is slightly lower than the predictions of the model. For the tensor constants, measured and predicted values agree to within about 1% for both the 10F and 10G states, though in each case the agreement is slightly outside the estimated combined errors of theory and experiment. In general, however, the measured structure of

TABLE VII. Determination of the structure factors A_0 and A_2 for the 10F and 10G states from measured level positions. Numbers in parentheses denote errors.

State	Position	Eq. (20)	Net	Fit
(0,1)10F ₂	-2.570(6)	-0.038(5)	-2.532(8)	$A_0 = -1.006(6)$
(0,1)10F ₄	-1.789(4)	-0.147(7)	-1.642(8)	$A_2 = -9.539(32)$
(0,1)10F ₃	0.750(2)	-0.152(1)	0.902(2)	
(0,1)10G ₃	-0.876(3)	-0.0096(1)	-0.866(3)	$A_0 = -0.2658(21)$
(0,1)10G ₅	-0.598(2)	-0.0267(1)	-0.571(2)	$A_2 = -4.200(15)$
(0,1)10G ₄	0.541(2)	-0.0318(1)	0.574(2)	

TABLE VIII. Comparison of measured scalar and tensor structure constants for the (0,1) $10F$ and (0,1) $10G$ states of H_2 with predictions of the polarization model. All values in cm^{-1} . Numbers in parentheses denote errors.

	$A_0(10F)$	$A_0(10G)$	$A_2(10F)$	$A_2(10G)$
LOPM	-1.0638	-0.2821	-9.4813	-4.2437
HOPM	-1.003(61)	-0.2777(44)	-9.471(10)	-4.2430(7)
obs	-1.006(6)	-0.2658(21)	-9.539(32)	-4.200(15)
obs/HOPM	1.003(61)	0.957(18)	1.007(3)	0.990(4)

(0,1) $10F$ and (0,1) $10G$ states agrees remarkably well with the predictions of the polarization model. The agreement is comparable to that found in analogous studies of the helium atom,¹¹ to this level in the theory.

Much higher spectroscopic precision, in states of higher L , will be possible in future studies of this system using microwave spectroscopy. The polarization model, complete through terms of order r_2^{-6} , will be increasingly precise when applied to states of higher L , as Table I illustrates. The precision of the polarization model could be further improved if all terms up to order r_2^{-8} could be calculated systematically, as has been done for helium.¹¹ Combined with advances in experimental precision, this

could lead to precise determination of the quadrupole moment and isotropic dipole polarizability of H_2^+ .

ACKNOWLEDGMENTS

This work was supported in part by the National Science Foundation under Grant Nos. PHY84-13123 and PHY87-09707. The authors are indebted to Richard Drachman and David Bishop for numerous helpful conversations, and to the latter for generously providing unpublished results of calculations in progress. David Van Baak, Phil Bontrager, and Francis Deck assisted in carrying out parts of the work described here.

¹W. G. Sturuss, P. E. Sobol, and S. R. Lundeen, Phys. Rev. Lett. **54**, 792 (1985).

²G. Herzberg and Ch. Jungen, J. Chem. Phys. **77**, 5876 (1982).

³E. E. Eyler, R. C. Short, and F. M. Pipkin, Phys. Rev. Lett. **56**, 2602 (1986).

⁴This corresponds to Hunds-case d coupling of the Rydberg electron to the internuclear axis. The core electron remains tightly coupled to the internuclear axis.

⁵W. G. Sturuss, E. A. Hessels, and S. R. Lundeen, Phys. Rev. Lett. **57**, 1863 (1986).

⁶Ch. Jungen and E. Miescher, Can. J. Phys. **47**, 1769 (1969).

⁷E. E. Eyler and F. M. Pipkin, Phys. Rev. A **27**, 2462 (1983).

⁸R. D. Knight and Liang-guo Wang, Phys. Rev. Lett. **55**, 1571 (1985).

⁹E. S. Chang, S. Pulchtopek, and E. E. Eyler, J. Chem. Phys. **80**, 601 (1984).

¹⁰R. Kachru and H. Helm, Phys. Rev. Lett. **55**, 1575 (1985).

¹¹R. J. Drachman, Phys. Rev. A **26**, 1228 (1982).

¹²S. L. Palfrey and S. R. Lundeen, Phys. Rev. Lett. **53**, 1141 (1984).

¹³In Ref. 5, the exchange energy of the (0,1) $10G_5$ states is measured to be 0.5 ± 0.1 MHz.

¹⁴L. D. Landau and E. M. Lifshitz, *Quantum Mechanics: Non-Relativistic Theory* (Addison-Wesley, Reading, MA, 1965), p. 297.

¹⁵A. R. Edmonds, *Angular Momentum in Quantum Mechanics* (Princeton University Press, Princeton, NJ, 1957), p. 55.

¹⁶U. Fano, Phys. Rev. A **2**, 353 (1970).

¹⁷E. E. Eyler, Phys. Rev. A **34**, 2881 (1986).

¹⁸M. Brieger, Chem. Phys. **89**, 275 (1984).

¹⁹D. M. Bishop and B. Lam, Chem. Phys. Lett. **134**, 283 (1987).

²⁰J. Schulman, R. Detrano, and J. I. Musher, Phys. Rev. A **5**, 1125 (1972).

²¹D. M. Bishop and L. M. Cheung, J. Phys. B **11**, 3133 (1978).

²²C. J. Kleinman, Y. Hahn, and L. Spruch, Phys. Rev. **165**, 53 (1968); J. Callaway, R. W. LaBahn, R. T. Pu, and W. M. Duxler, *ibid.* **168**, 12 (1968).

²³A. D. Buckingham, Adv. Chem. Phys. **12**, 107 (1967).

²⁴D. M. Bishop and G. Maroulis, J. Chem. Phys. **82**, 2380 (1985).

²⁵A. D. McLean and M. Yoshimine, J. Chem. Phys. **47**, 1927 (1967).

²⁶D. M. Bishop (private communication).

²⁷D. M. Bishop (private communication). The values reported are similar to those shown in Tables II and III of Ref. 19, except that the vibrational wave function corresponding to $R=1$, rather than $R=0$, was used to compute the average,

²⁸D. M. Bishop (private communication).

²⁹K. Bockasten, Phys. Rev. A **9**, 1087 (1974).

³⁰H. W. Kugel, M. Leventhal, D. E. Murmick, C. K. N. Patel, and O. R. Wood II, Phys. Rev. Lett. **35**, 647 (1975).

³¹F. R. Petersen, E. C. Beaty, and C. R. Pollack, J. Mol. Spectrosc. **102**, 112 (1983).

³²A. Dalgarno and J. T. Lewis, Proc. R. Soc. London, Ser. A **233**, 70 (1955).

³³G. Hunter, A. W. Yau, and H. O. Pritchard, At. Data Nucl. Data Tables **14**, 11 (1974).